Published in final edited form as:
Neuron. 2011 January 27; 69(2): 244–257. doi:10.1016/j.neuron.2010.12.016.

Nodes of Ranvier Act as Barriers to Restrict Invasion of Flanking Paranodal Domains in Myelinated Axons

Courtney Thaxton[1], **Anilkumar M. Pillai**[1], **Alaine L. Pribisko**[1], **Jeffrey L. Dupree**[2], and **Manzoor A. Bhat**[1,3,4,5,*]

[1]Department of Cell and Molecular Physiology, University of North Carolina, School of Medicine Chapel Hill, Chapel Hill, North Carolina 27599-7545

[2]Department of Anatomy and Neurobiology, Virginia Commonwealth University, Richmond, Virginia 23298-0709

[3]Neuroscience Center, University of North Carolina, School of Medicine Chapel Hill, Chapel Hill, North Carolina 27599-7545

[4]Curriculum in Neurobiology, University of North Carolina, School of Medicine Chapel Hill, Chapel Hill, North Carolina 27599-7545

[5]Carolina Institute for Developmental Disabilities, University of North Carolina, School of Medicine Chapel Hill, Chapel Hill, North Carolina 27599-7545

Abstract

Accumulation of voltage gated sodium (Na_v) channels at nodes of Ranvier is paramount for action potential propagation along myelinated fibers, yet the mechanisms governing nodal development, organization and stabilization remain unresolved. Here, we report that genetic ablation of the neuron-specific isoform of *Neurofascin* (*Nfasc*^{NF186}) *in vivo* results in nodal disorganization, including loss of Na_v channel and ankyrin-G (AnkG) enrichment at nodes in the peripheral (PNS) and central (CNS) nervous systems. Interestingly, the presence of paranodal domains failed to rescue nodal organization in the PNS and the CNS. Most importantly, using ultrastructural analysis, we demonstrate that the paranodal domains invade the nodal space in *Nfasc*^{NF186} mutant axons and occlude node formation. Our results suggest that Nfasc^{NF186}-dependent assembly of the nodal complex acts as a molecular boundary to restrict the movement of flanking paranodal domains into the nodal area, thereby facilitating the stereotypic axonal domain organization and saltatory conduction along myelinated axons.

Introduction

The sequestration of ion channels into molecularly distinct axonal domains is vital for nervous system function. Enrichment of voltage-gated sodium (Na_v) channels at nodes of Ranvier is of considerable importance, as they function to potentiate the nerve impulse in a saltatory manner along myelinated fibers (Rasband, 2006; Salzer, 2003; Thaxton and Bhat, 2009; Waxman and Ritchie, 1993). Recent findings have raised key questions concerning

[*]**Correspondence should be addressed to:** Manzoor A. Bhat, Neuroscience Center, NRB #5109, University of North Carolina School of Medicine, Chapel Hill, NC 27599-7545 Manzoor_Bhat@med.unc.edu.

the mechanisms regulating nodal development, such as whether nodes form independently of paranodes, or whether paranodes are sufficient for nodal organization. Neurofascins (Nfasc), a group of cell adhesion molecules with spatio-temporal expression in the nervous system, have been recently implicated in axonal function (Davis and Bennett, 1993; Tait et al., 2000; Volkmer et al., 1992). Two major isoforms have been characterized, the glial-specific $Nfasc^{NF155}$ (NF155) that localizes to the paranodes (Tait et al., 2000), and the neuron-specific $Nfasc^{NF186}$ (NF186) that is enriched at nodes of Ranvier and axon initial segments (Collinson et al., 1998; Davis et al., 1996; Hassel et al., 1997). Genetic ablation of *Nfasc* in mice ($Nfasc^{-/-}$) resulted in paranodal and nodal disorganization due to loss of both NF155 and NF186, and death at postnatal day 7, further highlighting their importance in myelinated axons (Sherman et al., 2005). While glial-specific loss of $Nfasc^{NF155}$ revealed its specific role in paranodal domain formation and stabilization (Pillai et al., 2009), the distinct *in vivo* role of NF186 in node of Ranvier organization and function is unclear.

Initial studies using shRNA knockdown of NF186 in neurons, *in vitro*, suggested that NF186 coordinates nodal formation and Na_v channel accumulation in PNS nodes independently of paranodes, but in an extrinsic manner, implying that external cues are required for node formation (Dzhashiashvili et al., 2007). Other studies performed in transgenic mice expressing $Nfasc^{NF186}$ in a $Nfasc^{-/-}$ mutant background, revealed that NF186 can facilitate nodal organization independently of paranodes, in both the CNS and PNS (Zonta et al., 2008). Interestingly, when $Nfasc^{NF155}$ was transgenically re-expressed in myelinating glia in the $Nfasc^{-/-}$ mutant background (mimicking NF186 loss), clustering of Na_v channels was observed at the CNS, but not the PNS nodes (Zonta et al., 2008). This data suggested that paranodal domains may suffice in organizing nodes in the absence of NF186 in the CNS. In contrast, *in vitro* studies utilizing Schwann cells and neurons isolated from wild type and $Nfasc^{-/-}$ mice, respectively, suggested that the paranodal domains were responsible for Na_v channel enrichment at mature nodes in the PNS, regardless of NF186 expression (Feinberg et al., 2010). These conflicting observations have further complicated our understanding of the precise role of NF186 in nodal development, and the mechanisms that regulate node formation. Here, using an *in vivo* genetic ablation approach, we demonstrate that NF186 is required for proper nodal organization and function independent of paranodes, and that paranodal domains are not sufficient for nodal coordination in the CNS or the PNS *in vivo*. Furthermore, in the absence of intact nodes of Ranvier, flanking paranodal domains invade the nodal space, indicating that NF186 plays a vital role in the organization and demarcation of nodes of Ranvier in myelinated axons.

Results

Neuron Specific Ablation of $Nfasc^{NF186}$

To specifically ablate $Nfasc^{NF186}$ from neurons, $Nfasc^{Flox}$ mice (Pillai et al., 2009) were crossed to mice expressing *Cre recombinase* (*Cre*) under the neuron-specific promoter, *Neurofilament light chain (Nefl-Cre*) (Leconte et al., 1994; Schweizer et al., 2002). When *Cre* is expressed, the *loxP* sites flanking exon 2 of *Nfasc* are excised, thereby causing a frameshift that results in a premature stop codon (red asterisks) in exon 4 (Fig. 1A and Fig. S1A). PCR amplification of genomic tail DNA was used to identify *Nfasc* wild type (+/+), heterozygous (+/*Flox*), and homozygous floxed (*Flox*) alleles, as well as *Cre* (Fig. 1B). To test the efficacy of *Nefl-Cre* excision of *Nfasc* during myelination, genomic DNA was isolated from postnatal day (P) 0, 3, 6, 11, 16, and 19 wild type (*Nefl-Cre;*$Nfasc^{+/+}$) and *Nefl-Cre;*$Nfasc^{Flox}$ spinal cords (Fig. 1C). PCR analysis using primers specifically recognizing the *Nfasc* ablation product (*Null*), showed recombination of the $Nfasc^{Flox}$ gene at P0 (birth), indicating early expression of *Cre* by the *Nefl* promoter. Phenotypic analysis revealed manifestation of paresis, ataxia, and motor coordination deficits in *Nefl-Cre;*$Nfasc^{Flox}$ mice (Movie S1). The *Nefl-Cre;*$Nfasc^{Flox}$ mice were significantly smaller

than their wild type (+/+) littermates (Fig. 1D-E) and on average survived to P20. In order to test the specificity of Cre expression in neurons, the *Nefl-Cre* mice were crossed to the reporter mouse strains, $Tau^{mGFP/LacZ}$ and $Rosa26R^{LacZ}$ ($R26R^{LacZ}$) (Hippenmeyer et al., 2005; Soriano, 1999). It is important to note that two reporter strains were used, as the $Tau^{mGFP/LacZ}$ line can only be expressed in neurons, while the $R26R^{LacZ}$ is designed to be expressed in any cell that expresses *Cre*. β-Galactosidase staining of *Nefl-Cre;*$Tau^{mGFP/LacZ}$ tissue displayed positive activity of the *Nefl* promoter specifically in the brain, spinal cord, and dorsal root ganglia (DRG) neurons as early as P0, suggesting that *Nefl-Cre* is active prior to myelination (Fig. S1). At P11, both *Nelf-Cre;*$R26R^{LacZ}$ and *Nefl-Cre;*$Tau^{mGFP/LacZ}$ mice showed robust neuron-specific expression in spinal cord and brain tissue, respectively, with no staining observed within the white matter tracts (Fig. S1). Furthermore, we observed an increase in the expression of *Nefl-Cre* with time, suggesting that *Nefl-Cre* is temporally and dynamically regulated in neurons.

To further test the specificity of *Nefl-Cre* expression in neurons, sciatic nerves (SN, not including the DRG), and spinal cords from P12 wild type (+/+), *Cnp-Cre;*$Nfasc^{Flox}$, and *Nefl-Cre;*$Nfasc^{Flox}$ mice were extracted, and immunoblotted with antibodies against Cre recombinase (Cre) and pan-Neurofascin (NFct). Immunoblots of P12 SN lysates revealed strong expression of Cre in the glial-specific *Cnp-Cre* lysates (*Cnp-Cre;*$Nfasc^{Flox}$), while both wild type (+/+) and *Nefl-Cre;*$Nfasc^{Flox}$ lysates were negative for Cre expression (Fig. 1F). These results are consistent with previous reports (Schweizer et al., 2002), and indicate that Schwann cells do not express *Nefl-Cre*. Furthermore, spinal cord lysates from the same mice showed a significant reduction in neuronal-NF186 expression in *Nefl-Cre;*$Nfasc^{Flox}$ mice compared to wild type (+/+), while glialNF155 expression remained unchanged (Fig. 1F). These results further confirm the specificity of *Nefl-Cre* expression in neurons alone. Next, immunoblot analysis of spinal cord lysates from P-3, 6, 12, and 19 wild type (+/+) and *Nefl-Cre;*$Nfasc^{Flox}$ age-matched littermates was carried out. A significant loss of NF186 was observed at P3 in *Nefl-Cre;*$Nfasc^{Flox}$ spinal cords and was sustained through P19, while NF155 expression increased with time in the *Nefl-Cre;*$Nfasc^{Flox}$ as in the wild type (+/+) spinal cord lysates (Fig. 1G). Cre expression was present as early as P3 and persisted through P19 in *Nefl-Cre;*$Nfasc^{Flox}$ spinal cords. Immunostaining of teased sciatic nerve fibers (Fig. 1H-K) and spinal cords (Fig. 1L-O) from wild type (+/+) and *Nefl-Cre;*$Nfasc^{Flox}$ mice using anti-FIGQY (a pan-Nfasc antibody) indicated specific loss of NF186 (red) from PNS and CNS nodes, while glial-NF155 (green) expression was not affected in the paranodal region (Fig. 1H′, I′). The paranodal and juxtaparanodal domains, defined by Caspr (blue) (Fig. 1J′, K′, N′, O′) and potassium channel (K_v1.1, red) (Fig. 1J, K, N, O) localization, respectively, remained unchanged and segregated in *Nefl-Cre;*$Nfasc^{Flox}$ nerves as in wild type (+/+) nerves, although the nodal region appeared to be reduced in the *Nefl-Cre;*$Nfasc^{Flox}$ mutant myelinated fibers. Together, these results demonstrate the efficacy and specificity of *Nefl-Cre* in ablating neuronal NF186 in CNS and PNS myelinated fibers.

Nodal Organization Is Dependent on $Nfasc^{NF186}$ in the PNS

To determine the effect(s) of NF186 loss on nodal development and organization, sciatic nerve fibers from P-3, 6, 11, and 14 wild type (+/+) and *Nefl-Cre;*$Nfasc^{Flox}$ mice were immunostained with antibodies against Na_v channels (pan-Na_v; red) and ankyrin G (AnkG; red), a nodal cytoskeletal adapter protein that stabilizes Na_v channels at the nodes (Bouzidi et al., 2002; Kordeli et al., 1995; Lemaillet et al., 2003; Malhotra et al., 2002). Paranodal Caspr (green) localization was also examined in order to assess whether paranodes could maintain nodal clustering in the absence of NF186 (blue). In addition, we examined the localization of the PNS specific proteins, NrCAM (Lustig et al., 2001), Gliomedin (Gldn) (Eshed et al., 2005), and the ezrin-binding phosphoprotein-50 (EBP50) (Melendez-Vasquez et al., 2004) (Fig. S2). Gldn and EBP50 comprise a unique set of nodal proteins that are

expressed within glia, and more specifically within the nodal microvilli of SCs in the PNS. Particular emphasis was concentrated on Gldn expression and localization, as Gldn has been shown to associate with NF186, *in vitro* (Eshed et al., 2005). In P3 wild type (+/+) sciatic nerves, NF186 (blue) was enriched at nodes where it colocalized with AnkG (Fig. 2A) and Na_v channels (Fig. 2I). While colocalization was apparent, we also observed a number of nodes that were NF186 positive, but lacked detectable accumulation of AnkG or Na_v channels at this time (data not shown). These results are consistent with previous findings suggesting that NF186 precedes AnkG and Na_v channel localization at nascent nodes (Lambert et al., 1997; Schafer et al., 2006). Paranodal Caspr (green) was also observed flanking most of the developing nodes at this time. As myelination progressed, NF186, AnkG and Na_v channels became more focally concentrated to the nodal region in wild type (+/+) nerves. Specific loss of NF186 was observed in *Nefl-Cre;Nfasc*^{Flox} sciatic nerve fibers at P3 (Fig.1B″ and Fig. S3B′), and persisted through P14 (Fig. 1H″ and Fig. S3H′). At P3, concomitant loss of AnkG (red; Fig. 1B′) and Na_v channel (red, Fig. 1J′) accumulation at nodes (arrowheads) lacking NF186 was observed in *Nefl-Cre;Nfasc*^{Flox} myelinated axons. However, the presence of paranodes in *Nefl-Cre;Nfasc*^{Flox} sciatic nerve fibers was not able to rescue Na_v channel or AnkG clustering at this stage, nor at P6-14. In addition, we frequently observed a progressive shortening of the nodal gap in the *Nefl-Cre;Nfasc*^{Flox} axons, compared to wild type (+/+). Furthermore, the PNS specific proteins, NrCAM, Gldn, and EBP50 also failed to accumulate in nodes of *Nefl-Cre;Nfasc*^{Flox} myelinated fibers compared to wild type (+/+) nerves (Fig. S2). Quantification revealed that 65% of nodes in P11 *Nefl-Cre;Nfasc*^{Flox} sciatic nerve fibers lacked NF186 expression compared to wild type fibers (Fig. 2Q). Of the nodes lacking NF186 expression, approximately 76% and 70% also lacked AnkG (Fig. 2Q′) and Na_v channel (Fig. 2Q″) expression, respectively. These findings indicate that NF186 is required for Na_v channel and AnkG localization and stabilization at the PNS nodes *in vivo*. Moreover, they demonstrate that flanking paranodal domains are not sufficient in assembling nodes in the absence of NF186 in the PNS.

Due to the significant loss of Na_v channel accumulation at nodes of *Nefl-Cre;Nfasc*^{Flox} axons, electrophysiological analysis was performed on sciatic/plantar nerves from P15 wild type (+/+) and *Nefl-Cre;Nfasc*^{Flox} mice. As anticipated, the conduction velocity (CV) in *Nefl-Cre;Nfasc*^{Flox} nerves (CV= 14.7 ± 2 SEM) was significantly reduced (p-value = 0.0202) compared to wild type nerves (CV= 22.6 ± 0.4) (n=3 for both). Complete loss of conduction velocity was not expected as *Nefl-Cre* does not completely ablate NF186 expression, as evident from the immunoblot analysis (Fig. 1F-G). Overall, the results suggest that NF186 coordinates nodal organization and the enrichment of both neuron- and glial-specific proteins to nodes in PNS myelinated axons.

Nfasc^{NF186} is Essential for Proper Nodal Organization in the CNS

Next, in order to assess the function of NF186 in CNS node development, spinal cord sections from wild type (+/+) and *Nefl-Cre;Nfasc*^{Flox} mice at P-3, 6, 11, and 14 were immunostained with antibodies against NF186, AnkG, Na_v channels and Caspr (Fig. 3). Similar to the PNS, NF186 accumulated in nodes of P3 wild type (+/+) mice (Fig. 3A″ and Fig. S3I″). AnkG (red; Fig. 3A′), and Na_v channels (red, Fig. 3I′) were also expressed in P3 wild type nodes, where they co-localized with NF186 (blue). During maturation (P6-14), NF186, AnkG and Na_v channel expression increased within developing nodes that were bordered by paranodal Caspr (green). Perturbation of NF186 expression in *Nefl-Cre;Nfasc*^{Flox} mice resulted in loss of AnkG and Na_v channel clustering in CNS nodes (arrowheads) at all time points, and decreased nodal length. Quantification revealed a significant increase in NF186 loss in nodes of P6 (80%; Fig. S4A), P11 (20%, Fig. 3Q), and P14 (55%, Fig. S4B) *Nefl-Cre;Nfasc*^{Flox} (gray bars) myelinated spinal cord fibers, compared to wild type (+/+, black bars) fibers. Furthermore, approximately 80% of the NF186 null

nodes also lacked AnkG (Fig. 3Q′ and Fig. S4A′, B′) and Na_v channel (Fig. 3Q″, and Fig. S4A″, B″) expression at the nodes. These results demonstrate that NF186 coordinates nodal formation by clustering AnkG and Na_v channels at the CNS nodes independent of the paranodes, as observed in the PNS.

Flanking Paranodal Domains Invade the Nodal Space in *Nfasc*^{NF186} Mutants

To date, only the paranodal domains are considered to act as molecular sieves to restrict the distribution of ion channels within myelinated axons (Pedraza et al., 2001; Salzer, 2003; Thaxton and Bhat, 2009). Indeed, several paranodal mutants exhibit juxtaparanodal potassium channel (K_v) redistribution in the absence of paranodal septate junctions (Salzer, 2003; Thaxton and Bhat, 2009). Yet, nodal components still assemble in nodes even in the absence of intact paranodal junctions, suggesting that nodes may also act as a barrier, or sieve, to restrict the mobility of molecules within the nodal region. From these earlier studies, as well as the decreased nodal length observed in *Nefl-Cre;Nfasc*^{Flox} myelinated fibers, we sought to determine the effect(s) of NF186 loss on the ultrastructural organization of nodes in myelinated axons. Electron microscopic (EM) analysis was carried out on the sciatic nerves from P15 wild type (+/+) and *Nefl-Cre;Nfasc*^{Flox} mice (Fig. 4). In wild type (+/+) sciatic nerves, the node is properly flanked by two adjacent paranodal glial domains (Fig. 4A), with septate-like junctions formed between the terminal myelin loops and the axolemma (Fig. 4C, arrowheads). Higher magnification of wild type (+/+) nerves revealed the presence of SC nodal microvilli (arrow) descending towards the nodal axolemma (Fig. 4C). The microvilli are unique to SCs and act to facilitate SC-axon and SC-SC communication within myelinated fibers. Nodal disorganization, including decreased nodal length, aberrant SC microvilli organization, and organelle accumulation (m) was observed in *Nefl-Cre;Nfasc*^{Flox} sciatic nerves (Fig. 4B, D-G) compared to wild type nerves (Fig. 4A,C). The SC nodal microvilli were disorganized in *Nefl-Cre;Nfasc*^{Flox} sciatic nerves and often appeared undifferentiated (Fig. 4D, arrows). Typically, the nodal length is ~1 μm (Rosenbluth, 2009), but measurements revealed a significant reduction (p-value = 0.0001) in nodal length, from 1.43μm (± 0.37 SEM, n=20) in wild type fibers to 0.72μm (± 0.16 SEM, n=30) in *Nefl-Cre;Nfasc*^{Flox} mutant fibers. Furthermore, closer examination revealed organelle accumulation (m; Fig. 4E), axolemmal constriction (arrows; Fig. 4N), septae formation (arrowheads; Fig. 4F), and SC microvillar invasion (asterisks; Fig. 4G) in the nodes of *Nefl-Cre;Nfasc*^{Flox} myelinated fibers. To assess whether reduction in the nodal gap occurred earlier in development, we performed EM analysis on P6 wild type (+/+) and *Nefl-Cre;Nfasc*^{Flox} sciatic nerves (Fig. 4H, I). Examination of the younger *Nefl-Cre;Nfasc*^{Flox} nerves revealed a similar phenotype as the P15 mutant nerves, including decreased nodal length (asterisk), aberrant SC nodal microvilli differentiation (arrows), organelle accumulation (m), and invasion of the adjacent paranodal loops (Fig. 4I). While it is apparent that the paranodes have initiated the invasion of the nodal region, the paranodal septae (arrowheads) were still intact and present in the *Nefl-Cre;Nfasc*^{Flox} myelinated fibers as in the wild type (+/+) nerves, suggesting that loss of nodal formation and organization does not affect the assembly of the paranodal domains (Fig. 4 H-I). Next, we wanted to assess the development and architecture of the SC nodal microvilli in P15 wild type (+/+) and *Nefl-Cre;Nfasc*^{Flox} sciatic nerves. Transverse sections through the nodes revealed an atypical arrangement of SC microvilli (arrows) in *Nefl-Cre;Nfasc*^{Flox} nerves (Fig. 4K-M) compared to wild type nerves (Fig. 4J), without any significant effects on myelination. The microvilli often ran parallel to, or everted away from the axon in *Nefl-Cre;Nfasc*^{Flox} myelinated sciatic nerve fibers, and were consistently observed with paranodal loops within the same section (Fig 4 K, M). The pinching of the nodal axolemma (Fig. 4M, arrowheads; Fig. 4N, arrows) and the presence of septate within the nodal region (Fig. 4O, arrowheads) was also observed in *Nefl-Cre;Nfasc*^{Flox} nerves. These nodal deformities, caused by the apparent paranodal invasion, were never observed in the wild type myelinated axons. Taken

together, these results demonstrate that loss of nodal formation and organization, in the absence of NF186, results in the invasion of the nodal space by the flanking paranodal domains.

Next, we examined the spinal cords of P6 and P15 wild type (+/+) and *Nefl-Cre;Nfasc*^{Flox} by EM analysis (Fig. 5). In the CNS, reduced nodal length (asterisks) was also observed in *Nefl-Cre;Nfasc*^{Flox} mice (Fig. 5B) compared to wild type (+/+; Fig. 5A), as in the PNS, while the paranodal axo-glial septae were still observed (arrowheads). Similarly, we observed the initial paranodal invasion of the nodal region in P6 *Nefl-Cre;Nfasc*^{Flox} myelinated axons (arrows, Fig. 5D) compared to wild type (+/+; Fig 5C). A perinodal astrocytic process (double arrows) was also observed invading the region between the overlapping paranodal domains in P6 *Nefl-Cre;Nfasc*^{Flox} nerves, even in the presence of intact paranodal septae (arrowheads; Fig. 5D). As the mice matured, nodal obstruction caused by overriding adjacent paranodal loops was frequently observed in P15 *Nefl-Cre;Nfasc*^{Flox} CNS fibers (Fig. 5E-H, arrows). Quantification revealed a significant (p-value = 0.0001) decrease in nodal length in *Nefl-Cre;Nfasc*^{Flox} nerves (0.57μm ± 0.05, n=29) compared to wild type nerves (1.12μm ± 0.04, n=49). This 50% reduction in nodal length in CNS myelinated fibers is consistent with the reduction observed in the PNS, suggesting that NF186 expression at nodes is critical for maintaining the proper nodal area in both the PNS and CNS. In addition, perinodal astrocytic processes (double arrows) often occupied the space between two overriding paranodal domains in P15 *Nefl-Cre;Nfasc*^{Flox} myelinated fibers, and is comparable to the invading SC microvilli observed in *Nefl-Cre;Nfasc*^{Flox} PNS nodes (compare Fig. 5E with Fig. 4G). Overall, these results are consistent with our light microscopic analysis and demonstrate that NF186 is essential for nodal complex assembly. Once assembled, this complex would act to prevent invasion of the nodal region by flanking paranodes, astrocytic processes (in the CNS), and SC nodal microvilli (in the PNS).

Organization of the Nodal Components Occurs Independent of Paranodes in the CNS and PNS

Key questions concerning the role of paranodes in nodal formation and organization have been raised, but conflicting evidence has hampered our understanding of the contribution of paranodes to nodal function (Zonta et al., 2008; Feinberg et al., 2010). To assess the role of paranodes in nodal organization, we immunostained sciatic nerve fibers and spinal cord sections from paranodal, nodal, and combined mutant mice with several domain specific antibodies (Fig. 6). In *Caspr* $^{-/-}$ (Fig. 6A) (Bhat et al., 2001) and *Cnp-Cre;Nfasc*^{Flox} (Fig. 6B) (Pillai et al., 2009) myelinated fibers, loss of the paranode-specific proteins Caspr and NF155, respectively, did not disrupt the localization and enrichment of NF186, AnkG, and Na_v channels at nodes in the PNS (a-f) or CNS (g-l). Redistribution of juxtaparanodal K_v channels (K_v1.1, green) within the paranodal space was also observed in the PNS and CNS of both paranodal mutants, and is consistent with previously published results (Dupree et al., 1999; Bhat et al., 2001; Pillai et al., 2009). In addition, we found that the localization of NrCAM, Gldn and EBP50 to nodes was unchanged in *Caspr*$^{-/-}$ and *Cnp-Cre;Nfasc*^{Flox} sciatic nerves compared to wild type nerves (Fig. S5A-B). Re-examination of P19 *Nefl-Cre;Nfasc*^{Flox} nerves revealed identical results as the earlier time points, including loss of AnkG and Na_v channel enrichment at PNS and CNS nodes (Fig. 6C), and loss of NrCAM, Gldn, and EBP50 localization at PNS nodes lacking NF186 expression, while paranodal Caspr and NF155 (NFct) expression was retained (Fig. S5C). As expected, in *Act-Cre;Nfasc*^{Flox} mice, which lack both NF155 and NF186, accumulation of AnkG and Na_v channels failed to occur at presumptive nodal sites, as well as Caspr at the paranodes in both the PNS and CNS (Fig. 6D). The clustering of the PNS specific nodal proteins NrCAM and Gldn was also disrupted in *Act-Cre;Nfasc*^{Flox} nerves compared to wild type (Fig. S5D). Taken together, these results clearly demonstrate that nodes form independent of paranodes

in vivo, and that intact paranodes are neither necessary nor sufficient to aid nodal assembly and organization in the absence of NF186, *in vivo* in both CNS and PNS myelinated axons.

Discussion

Proper assembly and clustering of Na_v channels within nodes of Ranvier is critical for nervous system function and homeostasis. Several molecules enriched at the node, including NF186, AnkG, and βIV-spectrin, have been implicated as potential regulators of Na_v channel localization, stabilization and function, but the exact mechanisms governing the initial formation and organization of nodes remains unclear. Here, we have presented *in vivo* evidence that the neuronal isoform of Nfasc, NF186, is critical for proper nodal development, organization and function in myelinated axons. Furthermore, we demonstrate that paranodal domains are not compensatory in clustering Na_v channels, or AnkG, at NF186 null nodes *in vivo*. Finally, we find that a NF186-dependent molecular complex at the nodes acts to demarcate the nodal region, thus preventing the occlusion of the node by its adjacent paranodal domains. Together, these findings provide significant insight into the mechanisms regulating nodal organization and axonal function, and may therefore provide clues about myelin-related pathologies that alter saltatory conduction in myelinated axons.

$Nfasc^{NF186}$ is the Organizer of Nodes of Ranvier in the PNS and CNS

Key questions regarding the mechanisms regulating nodal organization have been raised, including what protein(s) coordinate nodal organization, does it occur intrinsically or extrinsically, and what is the role of glia in the organization of nodes? Here we find that neuron-specific ablation of NF186, *in vivo*, results in disrupted nodal development, including the loss of Na_v channels and AnkG enrichment at nodes, severe conduction velocity delays, shortened nodal gaps, and death at P20. Disruption of Na_v channel clustering at nodes was observed as early as P3 in myelinated axons within the peripheral sciatic nerves (Fig. 2), as well as the central spinal cord white matter fibers (Fig. 3). In accordance, we also observed perturbation of AnkG, the cytoskeletal adaptor protein that is required for sodium channel stabilization at nodes, as well as NrCAM, and the PNS-specific glial expressed nodal proteins, Gldn and EBP50 (Fig. S2). Moreover, we consistently observed that, on average, 80% of NF186 negative nodes also lacked AnkG and Na_v channel expression throughout postnatal development (Figs. 2, 3 & S4). Together these findings indicate that *in vivo*, NF186 acts to coordinate nodal organization and development in myelinated fibers.

In support of our studies, *in vitro* knockdown-rescue experiments revealed that expression of NF186 in neurons facilitated the recruitment of AnkG and Na_v channels to nodes in SC-DRG neuron co-cultures (Dzhashiashvili et al., 2007). Interestingly, expression of NF186 constructs lacking the AnkG binding domain ($NF186^{\Delta ABD}$) in neurons of myelinated co-cultures retained the ability to target to nodes (Dzhashiashvili et al., 2007). This finding suggests that NF186 localization to nodes is independent of AnkG, and supports an extrinsic model of nodal development, in which glial-mediated signaling would facilitate the clustering of NF186 in pre-forming nodes. It was also reported that suppression of AnkG expression in neurons, *in vitro*, resulted in aberrant NF186 and Na_v channel enrichment at the nodes (Dzhashiashvili et al., 2007). Here, the absence of NF186 in AnkG-negative nodes could be attributed more to the loss of its stabilization, as opposed to its localization, in AnkG null neurons, as the co-cultures used were analyzed 2-4 weeks post myelin induction. This later time of analysis may have prevented observation of the initial accumulation, followed by the progressive destabilization of NF186 in these cultures. Further support for NF186-mediated nodal organization is evidenced by the finding that transgenically modified $Nfasc^{-/-}$ mice re-expressing NF186 specifically in neurons was able to induce clustering of

several nodal components, including AnkG, Na_v channels, and the cytoskeletal protein βIV-spectrin in the absence of paranodes (Zonta et al., 2008).

In addition to its role in organizing the node, we find that NF186 expression precedes AnkG and Na_v channel localization to nascent nodes. In P3 wild type myelinated fibers, we consistently observed robust and increased expression of NF186 compared to AnkG and Na_v channels in immature nodes of the PNS and CNS. This observation is consistent with previous reports, where NF186 expression was observed in nodes prior to other nodal components (Dzhashiashvili et al., 2007; Koticha et al., 2006; Lambert et al., 1997; Lustig et al., 2001). In contrast, other studies suggest that AnkG targets prior to NF186 in CNS nodes from the observation that 11% of P14 optic nerve nodes expressed AnkG in the absence of NF186 (Jenkins and Bennett, 2002). While informative, myelination within the optic nerve begins at P6, six days after the initiation of myelination in CNS spinal cord nerves, as well as PNS nerves, which begin at birth (Jessen and Mirsky, 2005; Tennekoon et al., 1977). Taking the time shift into consideration, as P14 in the optic nerve would correspond to P8 in the spinal cord, we find that disruption of NF186 expression in P6 *Nefl-Cre;Nfasc*^{Flox} nerves perturbs AnkG localization at CNS nodes (Fig. 3D-D‴). On average, 95% of the NF186 null nodes also lacked AnkG (Fig. S4), suggesting that NF186's initial localization is required for the recruitment of AnkG to nodes *in vivo*. Moreover, the evident lack of AnkG and Na_v channel accumulation in P3 *Nefl-Cre;Nfasc*^{Flox} nerves, which is an earlier time point than what was examined in optic nerves, further supports our conclusions (Fig. 3B′ and K′). It is possible that in a small subset of nerves, AnkG may function to coordinate nodal formation, as 5% of our NF186 null nodes at P6 retained AnkG expression, although the expression was often diffuse and showed paranodal localization (data not shown), similar to that observed in P9 optic nerves (Jenkins and Bennett, 2002). It is more likely that our observation of AnkG in nodes lacking NF186 may represent nodes that had lost NF186 after initial assembly. Therefore with time, AnkG and other nodal components would gradually diffuse out of the node, causing the disassembly of the nodal cytoskeletal complex, which in turn would lead to the apparent invasion of the nodal region by the flanking paranodal domains. Together, these findings point to a mechanism in which initial clustering of NF186 mediates recruitment and enrichment of AnkG, and in turn Na_v channels at newly forming nodes, thereby coordinating nodal organization in myelinated fibers. As myelination advances, the nodes would become progressively stabilized by interactions between AnkG, βIV-spectrin, and the local axonal cytoskeleton (Fig. 7A).

Orchestration of Nodal Organization is Independent of the Paranodal Domains

Recent reports have suggested that paranodes may suffice to induce clustering of nodal components in the absence of NF186, although there is great debate concerning the mechanisms regulating paranodal-induced nodal clustering, the proteins involved, and whether or not it occurs in the PNS, the CNS, or both. Here we demonstrate that *in vivo*, paranodes are not sufficient to rescue organization of the nodal components, AnkG and Na_v channels, in the absence of NF186 expression in both the CNS and PNS. We also find that lack of NF186 expression in the PNS perturbs the proper localization and stabilization of the SC-specific nodal microvilli proteins Gldn and EBP-50, and the neuronally expressed NrCAM. These results were consistently observed throughout postnatal development, from P3 to P19, and are in direct contradiction to two recent reports which suggest that paranodes rescue nodal organization in *Nfasc*^{NF186} transgenic null mutants, and in *in vitro* co-cultures (Zonta et al., 2008; Feinberg et al, 2010). In the case of Zonta et al., transgenic re-expression of NF155 potentially targeted to myelinating glia of *Nfasc*$^{-/-}$ mice, *in vivo*, was shown to enable clustering of Na_v channels at nodes, but only in the CNS and not the PNS. However, these mice only survived to P7, the same expiry as the *Nfasc*$^{-/-}$mice that lack both glial-NF155 and neuronal-NF186, indicating that the transgenic NF155 was not sufficient to

completely rescue nodal organization. Furthermore, the *proteolipid protein* (*Plp*) promoter was used to express NF155 in myelinating glia, which was recently shown to be expressed in a subset of CNS, but not PNS neurons (Miller et al., 2009). Thus, a possibility remains that leaky expression of the $Nfasc^{NF155}$ construct within CNS neuronal populations, even at undetectable levels, would likely induce clustering of Na_V channels at CNS nodes.

In regards to Feinberg et al. (2010), a reason for this discrepancy may be attributed to their experimental strategy and use of an *in vitro* cell culture system, as opposed to our *in vivo* genetic knockout approach. Studies using *in vitro* myelinating co-cultures, while informative, do not necessarily recapitulate the exact mechanisms occurring *in vivo*, as the developmental time line and cellular environment vary dramatically. Analysis performed in the *in vitro* myelinating co-cultures was noted to have occurred 12 days post myelin induction. In these co-cultures the accumulation of nodal proteins at the distal tips of myelinating SCs (termed heminodes) was assessed as the initial sign of node formation, and with contributions of the paranodes these heminodes would coalesce into mature nodes (Feinberg et al., 2010). The model put forth by Feinberg et al. (2010), based on *in vitro* co-culture studies involving wild type SCs and various mutant DRG neurons and a combination there of, suggested that initial clustering of nodal components at the heminodes in the PNS depends on Gldn, NrCAM and NF186, and is independent of the paranodes. Then a second step is proposed in which these heminodal components would be brought together by the flanking paranodes to form mature nodes. Our *in vivo* analysis of $Nefl\text{-}Cre;Nfasc^{Flox}$ nerve fibers failed to show significant accumulation of Na_V channels or AnkG in the absence of NF186 at all developmental stages in the PNS, indicating that intact paranodes do not act as a second step in node formation. Instead of clustering nodal components in the absence of NF186, the paranodes invaded the nodal space and obscured node formation in both the CNS and the PNS (Figs. 4 and 5). Given the differences in maturation of the *in vitro* myelinating co-cultures, compared to *in vivo* myelination, it is possible that overtime some clustering may be observed at putative nodal sites in wild type SC;$Nfasc^{-/-}$ neuron *in vitro* co-cultures, but the long-term stability of proteins within these nodes is unknown. Moreover, clustering of the nodal components in the absence of NF186 was neither observed by Zonta et al. (2008), nor in our studies in the PNS myelinated axons *in vivo*.

Further support for a paranode independent mechanism for node formation comes from earlier findings that nodes assemble in the absence of intact paranodes, as observed in $Caspr^{-/-}$ (Bhat et al., 2001), $Nfasc^{NF155\,-/-}$ ($Cnp\text{-}Cre;Nfasc^{Flox}$) (Pillai et al., 2009), $CGT^{-/-}$ (Dupree et al., 1999) and $Cont^{-/-}$ mutants (Boyle et al., 2001) (see Fig. 6 and Fig. S5). Overall, our results demonstrate that nodes form independent of paranodes and that *in vivo* intact paranodes are neither necessary nor sufficient to initiate, or rescue nodal assembly and organization in the absence of NF186, in both the CNS and the PNS myelinated axons (Fig. 7). Since *Nefl-Cre* expression is dynamically regulated and all neuronal populations do not express *Cre* at the same time, we followed the loss of NF186 from P3 on wards until P19. At every age point analyzed, including P3, we observed that in nodes that had no detectable trace of NF186, the paranodes were invading the nodal space. Coincidentally, if both paranodal NF155 and nodal NF186 were affected in $Nefl\text{-}Cre;Nfasc^{Flox}$ mice, we would not have been able to identify these nodal regions, as no paranodal or nodal proteins would be detected in this situation, similar to $Act\text{-}Cre;Nfasc^{Flox}$ mice (Fig. 6). Our results are consistent both in the PNS and the CNS and are clearly in variance with reports by Zonta et al. (2008) and Feinberg et al. (2010). The discrepancies between our spatio-temporal phenotypic analysis using the *in vivo* Cre-based knock out strategy combined with ultrastructural analysis, and the reported *in vitro* myelination assays are solely due to different experimental conditions used in the respective studies.

Maintaining Molecular Boundaries at Nodes of Ranvier

We and others have previously shown that paranodal axo-glial junctions act as a physical barrier to segregate nodal Na_v channels from juxtaparanodal K^+ channels (Dupree et al., 1999; Bhat et al., 2001; Pillai et al., 2009). Loss of the paranodal junctions results in the movement of the juxtaparanodal components towards the nodal region, while the nodal components essentially remain at the nodal site. Lack of nodal redistribution in the absence of intact paranodal septa suggests that the nodal components may be anchored externally by the glial processes, and/or internally by the nodal axonal cytoskeleton (Bhat et al., 2001; Rios et al., 2003). A significant and novel finding of the current study is that NF186 localization at the nodes of Ranvier is essential for the delineation and maintenance of the nodal gap, as loss of NF186 in *Nefl-Cre;Nfasc*^{Flox} mice resulted in progressive invasion of the nodal space by the flanking paranodal domains. Reduction of the nodal space was observed as early as P3 in the PNS and CNS, and progressed during myelination. EM analysis of P15 wild type and *Nefl-Cre;Nfasc*^{Flox} myelinated fibers revealed a 50-80% reduction in nodal length in PNS and CNS axons. Quite often nodes were found completely occluded by overlapping paranodal domains in the CNS of *Nefl-Cre;Nfasc*^{Flox} mice (Fig. 5E-H), indicating that the nodal complex acts as a molecular barrier to prevent the lateral mobility of the neighboring paranodes into the nodal space. Moreover, invasion of the nodal region often resulted in disrupted axo-glial junctions in the overlapping paranodal domains of P15 *Nefl-Cre;Nfasc*^{Flox} myelinated axons, suggesting that long-term paranodal stabilization may be dependent on proper nodal organization and maintenance. Consequently, long-term stabilization of the nodes may also be dependent on proper organization of the flanking paranodal domains (Rios et al., 2003). However, it remains to be established whether the paranodal domains would eventually invade the nodal region in *in vitro* co cultures reported in Feinberg et al. (2010). Consistent with our findings, nodes in P6 *Nefl-Cre;Nfasc*^{Flox} mice were shorter than their wild type counterparts. But, unlike the apparent paranodal disorganization observed in P15 *Nefl-Cre;Nfasc*^{Flox} axons, paranodes of P6 *Nefl-Cre;Nfasc*^{Flox} were often found abutting each other within the nodal space, not overlapping one another (Figs. 4 and 5). In fact, the formation of paranodal axo-glial junctions was almost identical between the *Nefl-Cre;Nfasc*^{Flox} and wild type myelinated axons, and further demonstrates the specificity of *Nefl-Cre* expression in neurons and not myelinating glia. These results suggest that during early development in *Nefl-Cre;Nfasc*^{Flox} mice, paranodal formation and organization occurs normally, even in the absence of NF186 expression and properly organized nodes. As *Nefl-Cre;Nfasc*^{Flox} mice mature, the adjacent paranodal domains begin to migrate into the nodal region first, before gradually invading the neighboring paranodal region. Continued lateral mobility of the flanking paranodal domains ultimately results in axonal domain disorganization, including disrupted paranodal axo-glial junctions, as well as pinching of the nodal axolemma. Thus, NF186 acts to delineate the nodal region by coordinating the organization and assembly of several transmembrane and cytoskeletal proteins into a unique molecular domain, which is then further stabilized by interactions with the glial processes overlying the nodal region. These mechanisms point to an independent, and not interdependent, assembly of the nodal complex *in vivo*, which once established, serves as a molecular fence to maintain distinct boundaries to facilitate saltatory conduction along myelinated fibers.

Experimental Procedures

Animals

All procedures involving mice were carried out under *UNC-IACUC* approved guidelines for the ethical treatment of laboratory animals. The *Nefl-Cre* mice were generously provided by Dr. Michael Sendtner (University of Wurzburg, Germany) and were previously described (Schweizer et al., 2002). The *Cnp-Cre;Nfasc*^{Flox} and the *Caspr*$^{-/-}$ were previously

described (Pillai et al., 2009; Bhat et al., 2001). The *Tau*$^{mGFP/LacZ}$ mice (Hippenmeyer et al., 2005) were provided by Dr. William Snider (University of North Carolina, USA). The *Rosa26R*^{LacZ} (*R26R*^{lacZ}) mice were generously provided by Dr. Victoria Bautch (University of North Carolina, USA). The β*Actin-Cre* (*Act-Cre*) mice were obtained from Jackson Labs (Maine, USA).

Conditional Targeting of the Nfasc Gene

The *Nfasc*^{Flox} mice used in this study were previously generated and described (Pillai et al., 2009). For extraction of genomic DNA from tail and spinal cord samples, the REDExtract-NAmp Tissue PCR kit was used according to the manufacturer's directions (Sigma-Aldrich, USA). Primers used include: *Nfasc* primer forward primer 1, 5′- TTT CTG ACT GTT CTG GGT GAC-3′, and reverse primer 2, 5′- GCT ACG ATG TAT CAT TTG GCA G-3′, and the *Null* forward primer 3, 5′-TTT ACG GTA TCG CCG CTC CCG ATT-3′, and the *Null* reverse primer 4, 5′- CCC TGT TCT GCT CCT GGT TCA GTC-3′. For *Cre*, we used the primers previously described (Pillai et al., 2009).

Antibodies and Reagents

The following antisera were previously described: guinea pig and rabbit anti-Caspr (Bhat et al., 2001), guinea pig anti-NF186 (recognizing the mucin domain) and rat anti-pan Neurofascin (NFct, recognizing the C-terminus) (Pillai et al., 2009); rabbit anti-Caspr2; rat anti-Ankyrin G (AnkG) (Thaxton et al., 2010). Additional primary antibodies used include: mouse anti-pan sodium channel (pan-Na_V), mouse anti-Dystrophin (Dp116, MANDRA1), mouse anti-Actin (Act) and mouse anti potassium channel (K_V1.1) from Sigma; rabbit anti-neuronal cell adhesion molecule (NrCAM), rabbit anti-ezrin binding protein 50 (EBP50), rabbit anti-Gliomedin (Gldn), and mouse anti-myelin basic protein (MBP) from Abcam. Mouse anti- βTubulin (Tub) was obtained from Cell Signaling. Rabbit anti-FIGQY was generously provided by Dr. Matt Rasband (Baylor College of Medicine, USA). All of the fluorescent secondary antibodies (AlexaFlour) were purchased from Molecular Probes (USA). The horseradish peroxidase (HRP)-conjugated secondary antibodies were purchased from Jackson Immunologicals (USA).

Tissue Preparation and Immunostaining

All tissue preparation was carried out essentially as described previously (Bhat et al, 2001; Pillai et al., 2009; Thaxton et al., 2010). Briefly, sciatic nerves (SN) harvested from anesthetized mice were fixed in 4% paraformaldehyde (in PBS) for 15-30 min at 4°C, followed by extensive washing in PBS (phosphate buffered saline). The SNs were subsequently teased onto slides and dried overnight. The teased SNs were subjected to permeabilization in ice cold acetone for 15 minutes followed by washing in PBS, and were blocked in buffer (5% BSA, 1% NGS, and 0.2% TX-100, in PBS) for 1 hour. The SNs were incubated with primary antibodies overnight in blocking buffer, followed by rinsing in PBS before being incubated with secondary antibodies for 1 hour at room temperature (RT). Finally, the SNs were mounted in VectaSheild (VectorLabs), before imaging. Spinal cord (SC) tissue was prepared as follows: mice were anesthetized and pericardially perfused with 4% paraformaldehyde (in PBS). The SC was removed and either subjected to post-fixation in 4% paraformaldehyde overnight at 4°C or washed in PBS. Following post-fixation the SCs were washed in PBS, and sliced using a Vibratome (Leica), to 30μm in thickness. The SC sections, were blocked as described above, and incubated with primary antibodies overnight at 4°C with shaking, washed and subjected to secondary antibodies. All images were acquired under identical settings using a Bio-Rad Radiance 2000 confocal microscope with Zeiss software as previously described (Thaxton et al., 2010), or an Axiovert scanning confocal microscope using Zeiss LSM510 software.

Immunoblotting

SNs and SCs from age matched wild type (+/+) and *Nefl-Cre;Nfasc*^{Flox}, and *Cnp-Cre;Nfasc*^{Flox} mice were harvested and frozen at −80°C until processing. The extraction was performed as follows: tissues were homogenized in lysis buffer (50mM Tris-HCl pH 7.5, 150mM NaCl, , 10mM EDTA pH 8.0, 1% SDS, 1% Triton X-100, and a protease inhibitor cocktail tablet), by 25-50 stokes using a glass mortar and pestle. The homogenates were incubated 45 min on ice with occasional mixing. The resulting lysates were centrifuged at 13,000 rpm for 20 min at 4°C, and the supernatant collected. Protein concentration was determined by Lowry Assay (BC assay, BIORAD), and equal amounts of protein were resolved by SDS-PAGE, followed by transfer of the proteins onto nitrocellulose membranes. The membranes were then blocked (5% non-fat dry milk, in PBS with 0.1% Tween-20 (PBS-T)), incubated with primary antibodies for 1 hr at RT or overnight at 4°C, then washed in PBS-T before secondary antibodies were applied for 40 min at RT. The membranes were washed further in PBS-T before chemiluminescent substrate was applied. The membranes were then exposed to autoradiographic film to obtain a signal.

Transmission Electron Microscopy (TEM)

TEM of P15 and P6 age-matched wild type (+/+) and *Nefl-Cre;Nfasc*^{Flox} littermates was carried out as described previously (Pillai et al., 2009; Thaxton et al., 2010). For quantification of the nodal length, the nodes from two independent wild type (+/+) and *Nefl-Cre;Nfasc*^{Flox} mice at P15 were measured, and the averages were calculated. See Quantification of Percentages and statistics below.

Electrophysiology

The conduction velocity measurements were carried out on three individual wild type (+/+) and *Nefl-Cre;Nfasc*^{Flox} mice as described previously (Pillai et al., 2009; Thaxton et al., 2010).

Quantification of Percentages and Statistics

For the quantification of the percent of nodes lacking NF186 expression for P6, P11, and P14 spinal cords, and P11 sciatic nerves, three independent wild type (+/+) and *Nefl-Cre;Nfasc*^{Flox} age-matched littermate mice were processed according to the methods above. The sections were immunostained with antibodies against paranodal Caspr and nodal NF186, in combination with either AnkG or Na_v channels. Three images per immunostained sections were acquired by the use of a Bio-Rad Radiance 2000 confocal microscope, at 63x magnification. The number of paranodes was calculated for each individual scan, for every animal. The number of nodes lacking NF186 alone, lacking both NF186 and AnkG, and those lacking NF186 and Na_v channels were counted. For the calculation of nodes lacking NF186 alone, the percentages were based on the total number of paranodes in the field of view. For the calculation of the number of nodes lacking NF186, and either AnkG or Na_v channels, the percentages were based on the number of NF186 negative nodes per field of view (Fig. S6). The percentages for all scans per animal were averaged, and the error bars represent the standard error of the mean (SEM). A standard t-test was used to calculate the statistical significance (p-value) between the percent of nodes in wild type mice compared to *Nefl-Cre;Nfasc*^{Flox} mice (GraphPad).

Supplementary Material

Refer to Web version on PubMed Central for supplementary material.

Acknowledgments

We are grateful to Michael Sendtner, William Snider, Klaus Nave and Victoria Bautch for generously sharing the *Nefl-Cre*, *Tau*$^{mGFP/LacZ}$, *Cnp-Cre* and *R26R*^{LacZ} mice, respectively, and Matt Rasband for sharing the anti-FIGQY antibody. We thank Alan Fanning, Alex Gow, Lori Isom and Stephen Lambert for comments on the manuscript, and Matt Rasband for helpful discussions. We also thank anonymous reviewers for their many insightful comments and suggestions, which led to a broader discussion of our *in vivo* findings. This work was supported by NIH grants GM063074 and NS050356, the National Multiple Sclerosis Society and the State of North Carolina (M.A.B).

REFERENCES

Bhat MA, Rios JC, Lu Y, Garcia-Fresco GP, Ching W, Martin M, Li J, Einheber S, Chesler M, Rosenbluth J. Axon-glia interactions and the domain organization of myelinated axons requires neurexin IV/Caspr/Paranodin. Neuron. 2001; 30:369–383. [PubMed: 11395000]

Bouzidi M, Tricaud N, Giraud P, Kordeli E, Caillol G, Deleuze C, Couraud F, Alcaraz G. Interaction of the Nav1.2a subunit of the voltage-dependent sodium channel with nodal ankyrinG. In vitro mapping of the interacting domains and association in synaptosomes. J. Biol. Chem. 2002; 277:28996–29004. [PubMed: 12036953]

Boyle ME, Berglund EO, Murai KK, Weber L, Peles E, Ranscht B. Contactin orchestrates assembly of the septate-like junctions at the paranode in myelinated peripheral nerve. Neuron. 2001; 30:385–397. [PubMed: 11395001]

Collinson JM, Marshall D, Gillespie CS, Brophy PJ. Transient expression of neurofascin by oligodendrocytes at the onset of myelinogenesis: implications for mechanisms of axon-glial interaction. Glia. 1998; 23:11–23. [PubMed: 9562181]

Davis JQ, Bennett V. Ankyrin-binding activity of nervous system cell adhesion molecules expressed in adult brain. J. Cell Sci. Suppl. 1993; 17:109–117. [PubMed: 8144685]

Davis JQ, Lambert S, Bennett V. Molecular composition of the node of Ranvier: identification of ankyrin-binding cell adhesion molecules neurofascin (mucin+/third FNIII domain-) and NrCAM at nodal axon segments. J. Cell Biol. 1996; 135:1355–1367. [PubMed: 8947556]

Dupree JL, Girault JA, Popko B. Axo-glial interactions regulate the localization of axonal paranodal proteins. J. Cell Biol. 1999; 147:1145–1152. [PubMed: 10601330]

Dzhashiashvili Y, Zhang Y, Galinska J, Lam I, Grumet M, Salzer JL. Nodes of Ranvier and axon initial segments are ankyrin G-dependent domains that assemble by distinct mechanisms. J. Cell Biol. 2007; 177:857–870. [PubMed: 17548513]

Eshed Y, Feinberg K, Poliak S, Sabanay H, Sarig-Nadir O, Spiegel I, Bermingham JR Jr. Peles E. Gliomedin mediates Schwann cell-axon interaction and the molecular assembly of the nodes of Ranvier. Neuron. 2005; 47:215–229. [PubMed: 16039564]

Feinberg K, Eshed-Eisenbach Y, Frechter S, Amor V, Salomon D, Sabanay H, Dupree JL, Grumet M, Brophy PJ, Shrager P. A glial signal consisting of gliomedin and NrCAM clusters axonal Na+ channels during the formation of nodes of Ranvier. Neuron. 2010; 65:490–502. [PubMed: 20188654]

Hassel B, Rathjen FG, Volkmer H. Organization of the neurofascin gene and analysis of developmentally regulated alternative splicing. J. Biol. Chem. 1997; 272:28742–28749. [PubMed: 9353344]

Hippenmeyer S, Vrieseling E, Sigrist M, Portmann T, Laengle C, Ladle DR, Arber S. A developmental switch in the response of DRG neurons to ETS transcription factor signaling. PLoS Biol. 2005; 3:e159. [PubMed: 15836427]

Jenkins SM, Bennett V. Developing nodes of Ranvier are defined by ankyrin-G clustering and are independent of paranodal axoglial adhesion. Proc. Natl. Acad. Sci. U. S. A. 2002; 99:2303–2308. [PubMed: 11842202]

Jessen KR, Mirsky R. The origin and development of glial cells in peripheral nerves. Nat Rev Neurosci. 2005; 6:671–682. [PubMed: 16136171]

Kordeli E, Lambert S, Bennett V. AnkyrinG. A new ankyrin gene with neural-specific isoforms localized at the axonal initial segment and node of Ranvier. J. Biol. Chem. 1995; 270:2352–2359. [PubMed: 7836469]

Koticha D, Maurel P, Zanazzi G, Kane-Goldsmith N, Basak S, Babiarz J, Salzer J, Grumet M. Neurofascin interactions play a critical role in clustering sodium channels, ankyrin G and beta IV spectrin at peripheral nodes of Ranvier. Dev. Biol. 2006; 293:1–12. [PubMed: 16566914]

Lambert S, Davis JQ, Bennett V. Morphogenesis of the node of Ranvier: co-clusters of ankyrin and ankyrin-binding integral proteins define early developmental intermediates. J. Neurosci. 1997; 17:7025–7036. [PubMed: 9278538]

Leconte L, Semonin O, Zvara A, Boisseau S, Poujeol C, Julien JP, Simonneau M. Both upstream and intragenic sequences of the human neurofilament light gene direct expression of lacZ in neurons of transgenic mouse embryos. J. Mol. Neurosci. 1994; 5:273–295. [PubMed: 7577369]

Lemaillet G, Walker B, Lambert S. Identification of a conserved ankyrin-binding motif in the family of sodium channel alpha subunits. J. Biol. Chem. 2003; 278:27333–27339. [PubMed: 12716895]

Lustig M, Zanazzi G, Sakurai T, Blanco C, Levinson SR, Lambert S, Grumet M, Salzer JL. Nr-CAM and neurofascin interactions regulate ankyrin G and sodium channel clustering at the node of Ranvier. Curr. Biol. 2001; 11:1864–1869. [PubMed: 11728309]

Malhotra JD, Koopmann MC, Kazen-Gillespie KA, Fettman N, Hortsch M, Isom LL. Structural requirements for interaction of sodium channel beta 1 subunits with ankyrin. J. Biol. Chem. 2002; 277:26681–26688. [PubMed: 11997395]

Melendez-Vasquez CV, Einheber S, Salzer JL. Rho kinase regulates schwann cell myelination and formation of associated axonal domains. J. Neurosci. 2004; 24:3953–3963. [PubMed: 15102911]

Miller MJ, Kangas CD, Macklin WB. Neuronal expression of the proteolipid protein gene in the medulla of the mouse. J. Neurosci. Res. 2009; 87:2842–2853. [PubMed: 19479988]

Pedraza L, Huang JK, Colman DR. Organizing principles of the axoglial apparatus. Neuron. 2001; 30:335–344. [PubMed: 11394997]

Pillai AM, Thaxton C, Pribisko AL, Cheng JG, Dupree JL, Bhat MA. Spatiotemporal ablation of myelinating glia-specific neurofascin (Nfasc NF155) in mice reveals gradual loss of paranodal axoglial junctions and concomitant disorganization of axonal domains. J. Neurosci. Res. 2009; 87:1773–1793. [PubMed: 19185024]

Rasband MN. Neuron-glia interactions at the node of Ranvier. Results Probl. Cell Differ. 2006; 43:129–149. [PubMed: 17068970]

Rios JC, Rubin M, Martin M, Downey RT, Einheber S, Rosenbluth J, Levinson SR, Bhat M, Salzer JL. Paranodal interactions regulate expression of sodium channel subtypes and provide a diffusion barrier for the node of Ranvier. J. Neurosci. 2003; 23:7001–7011. [PubMed: 12904461]

Rosenbluth J. Multiple functions of the paranodal junction of myelinated nerve fibers. J. Neurosci. Res. 2009; 87:3250–3258. [PubMed: 19224642]

Salzer JL. Polarized domains of myelinated axons. Neuron. 2003; 40:297–318. [PubMed: 14556710]

Schafer DP, Custer AW, Shrager P, Rasband MN. Early events in node of Ranvier formation during myelination and remyelination in the PNS. Neuron Glia Biol. 2006; 2:69–79. [PubMed: 16652168]

Schweizer U, Gunnersen J, Karch C, Wiese S, Holtmann B, Takeda K, Akira S, Sendtner M. Conditional gene ablation of Stat3 reveals differential signaling requirements for survival of motoneurons during development and after nerve injury in the adult. J. Cell Biol. 2002; 156:287–297. [PubMed: 11807093]

Sherman DL, Tait S, Melrose S, Johnson R, Zonta B, Court FA, Macklin WB, Meek S, Smith AJ, Cottrell DF. Neurofascins are required to establish axonal domains for saltatory conduction. Neuron. 2005; 48:737–742. [PubMed: 16337912]

Soriano P. Generalized lacZ expression with the ROSA26 Cre reporter strain. Nat. Genet. 1999; 21:70–71. [PubMed: 9916792]

Tait S, Gunn-Moore F, Collinson JM, Huang J, Lubetzki C, Pedraza L, Sherman DL, Colman DR, Brophy PJ. An oligodendrocyte cell adhesion molecule at the site of assembly of the paranodal axo-glial junction. J. Cell Biol. 2000; 150:657–666. [PubMed: 10931875]

Tennekoon GI, Cohen SR, Price DL, McKhann GM. Myelinogenesis in optic nerve. A morphological, autoradiographic, and biochemical analysis. J. Cell Biol. 1977; 72:604–616. [PubMed: 138685]

Thaxton C, Bhat MA. Myelination and regional domain differentiation of the axon. Results Probl. Cell Differ. 2009; 48:1–28. [PubMed: 19343313]

Thaxton C, Pillai AM, Pribisko AL, Labasque M, Dupree JL, Faivre-Sarrailh C, Bhat MA. In vivo deletion of immunoglobulin domains 5 and 6 in neurofascin (Nfasc) reveals domain-specific requirements in myelinated axons. J. Neurosci. 2010; 30:4868–4876. [PubMed: 20371806]

Volkmer H, Hassel B, Wolff JM, Frank R, Rathjen FG. Structure of the axonal surface recognition molecule neurofascin and its relationship to a neural subgroup of the immunoglobulin superfamily. J. Cell Biol. 1992; 118:149–161. [PubMed: 1377696]

Waxman SG, Ritchie JM. Molecular dissection of the myelinated axon. Ann. Neurol. 1993; 33:121–136. [PubMed: 7679565]

Zonta B, Tait S, Melrose S, Anderson H, Harroch S, Higginson J, Sherman DL, Brophy PJ. Glial and neuronal isoforms of Neurofascin have distinct roles in the assembly of nodes of Ranvier in the central nervous system. J. Cell Biol. 2008; 181:1169–1177. [PubMed: 18573915]

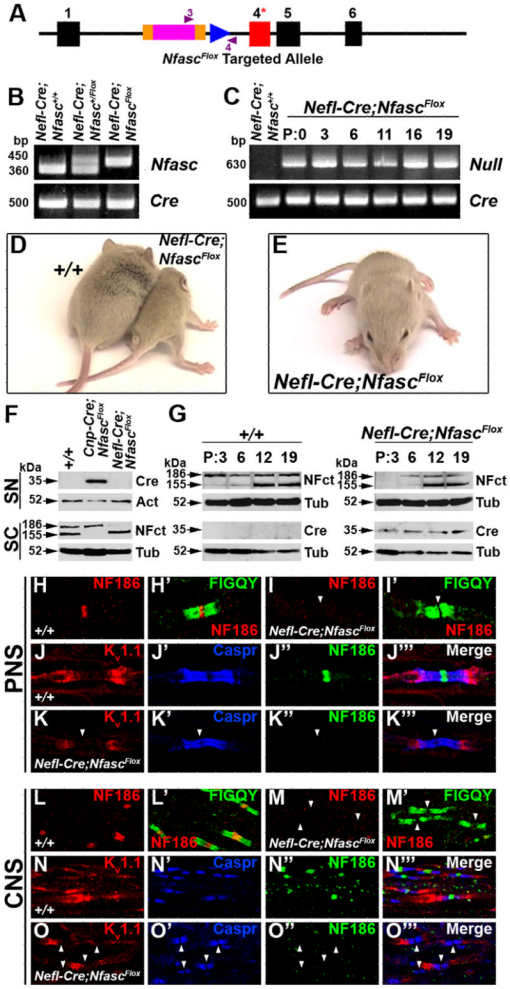

Figure 1. Generation of Neuron-specific *Nfasc*^{NF186} null mice

(A) Schematic diagram depicting the generation of the *Nfasc*^{Flox} allele (Pillai et al., 2009). **(B)** PCR amplification of genomic tail DNA isolated from wild type (*Nfasc*$^{+/+}$), heterozygous (*Nfasc*$^{+/Flox}$) and homozygous floxed (*Nfasc*^{Flox}) mice, and *Cre*. **(C)** PCR amplification of genomic DNA isolated from the spinal cords of postnatal day (P) 0, 3, 6, 11, 16, 19 *Nefl-Cre;Nfasc*^{Flox} and wild type (*Nefl-Cre;Nfasc*$^{+/+}$) mice using specific primers recognizing the excision product of the *Nfasc* allele (*Null*; primers 3 and 4 in A). **(D, E)** Photographic depiction of wild type (+/+) and *Nefl-Cre;Nfasc*^{Flox} mice. **(F)** Immunoblot analysis of sciatic nerve and spinal cord lysates from P12 wild type (+/+), *Cnp-Cre;Nfasc*^{Flox}, and *Nefl-Cre;Nfasc*^{Flox} mice with antibodies against Cre, Actin (Act; as a control), pan-Neurofascin (NFct), and tubulin (Tub; as a control). **(G)** Immunoblot analysis of spinal cord lysates from P-3, 6, 12, and 19 age matched wild type (+/+) and *Nefl-Cre;Nfasc*^{Flox} littermates with antibodies against NFct, Cre and Tub. Immunostaining of teased sciatic nerve fibers **(H-K)** and cervical spinal cord sections **(L-O)** from P15 wild type (+/+) and *Nefl-Cre;Nfasc*^{Flox} littermates with antibodies against panNeurofascin (FIGQY, green; **H′, I′, L′, M′**), NF186 (red in **H-I** and **L-M** ; green in **J-K** and **NO**), juxtaparanodal potassium channels (K_V1.1; red in **J-K** and **N-O**), and paranodal Caspr (blue in **J-K** and **N-O**). The asterisk (red) marks the insertion of a premature stop codon in exon 4 of *Nfasc*. Arrowheads indicate nodes lacking NF186. (See also Fig. S1).

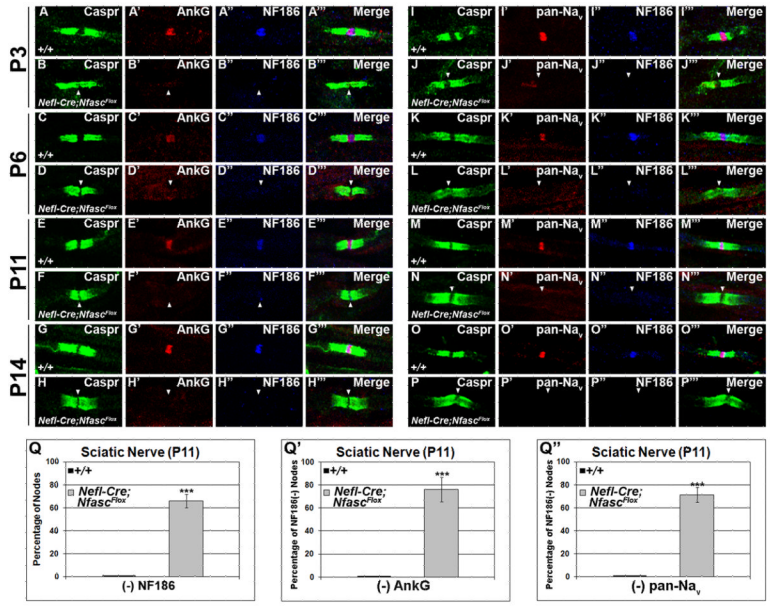

Figure 2. NF186 is required for node of Ranvier formation in the PNS

Sciatic nerve fibers from P3 (**A-B, I-J**), P6 (**C-D; K-L**), P11 (**E-F; M-N**), and P14 (**G-H; O-P**) age-matched wild type (+/+) and *Nefl-Cre;Nfasc*^{Flox} littermate mice were immunostained with antibodies against NF186 (blue), AnkG (red, **A′-H′**), and Na_v channels (pan-Na_v, red; **I′-P′**) where noted, plus Caspr (green). Arrowheads mark the nodes lacking NF186 expression in the *Nefl-Cre;Nfasc*^{Flox} mice. **(Q-Q″)** Quantification of the percentage of nodes lacking NF186 alone (-NF186, **Q**), lacking NF186 and AnkG (**Q′**), and those lacking NF186 and Na_v channels (**Q″**) in P11 wild type (+/+, black bars) and *Nefl-Cre;Nfasc*^{Flox} (gray bars) sciatic nerves. The calculation of nodes lacking both NF186 and AnkG [(−) AnkG] (**Q′**) or both NF186 and Na_v channels [(−) pan-Na_v] (**Q″**) are represented by the percent nodes lacking both proteins in relation to the total number of nodes lacking NF186. The graphs represent the average percent from three independent experiments, and the error bars represent the standard error of the mean (SEM). Asterisks (***) denote statistical significance with a p-value ≤ 0.0001. (See also Figs. S2 & S3).

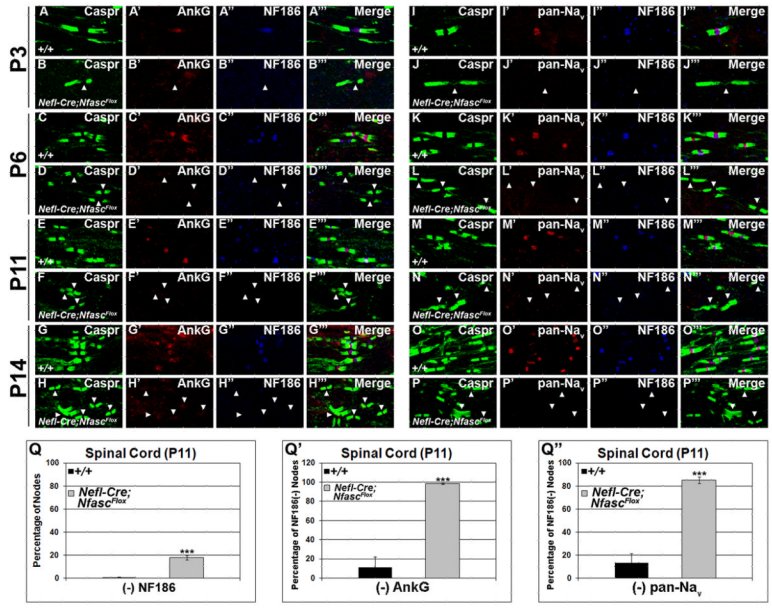

Figure 3. CNS node of Ranvier organization requires NF186

Cervical spinal cord sections from P3 (**A-B, I-J**), P6 (**C-D; K-L**), P11 (**E-F; M-N**), and P14 (**GH; O-P**) wild type (+/+) and *Nefl-Cre;Nfasc*^{Flox} age-matched littermate mice were immunostained with antibodies against Caspr (green), AnkG (red, **A′-H′**) or Na_v channels (panNa_v, red; **I′-P′**) where noted, plus NF186 (blue). Arrowheads mark the nodes lacking NF186 expression in the *Nefl-Cre;Nfasc*^{Flox} mice. **(Q-Q″)** Quantification of the percentage of nodes lacking NF186 alone (-NF186, **Q**), lacking both NF186 and AnkG (**Q′**), and those lacking both NF186 and Na_v channels (**Q″**) in P11 wild type (+/+, black bars) and *Nefl-Cre;Nfasc*^{Flox} (gray bars) spinal cords. The percentage of nodes lacking both NF186 and AnkG [(−) AnkG] (**Q′**) or both NF186 and Na_v channels [(−) pan-Na_v] (**Q″**) are represented by the percent nodes lacking both proteins in relation to the total number of nodes lacking NF186. The graphs represent the average percentages calculated from three independent experiments, and the error bars represent the SEM. Asterisks (***) denote statistical significance with a p-value ≤ 0.0001. (See also Figs. S2, S3 and S6).

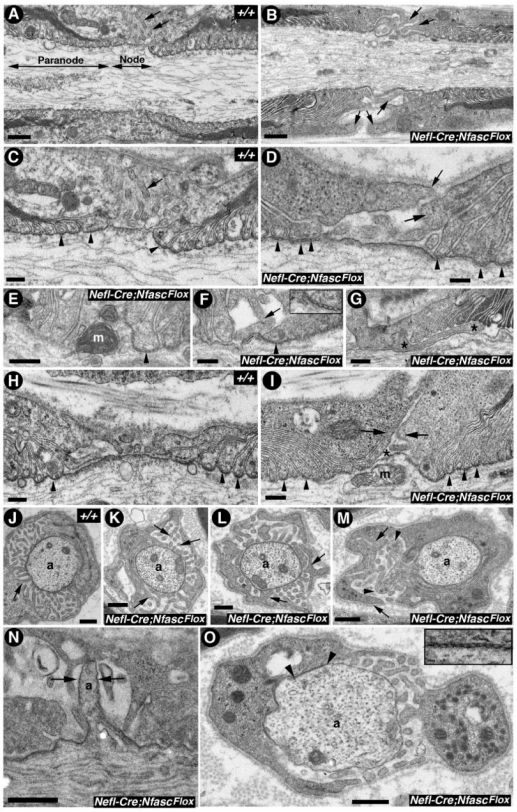

Figure 4. Invasion of the nodal region by flanking paranodal domains in the PNS of *Nfasc*^{NF186} null myelinated axons

Electron microscopic analysis of P15 (**A-G, J-O**) and P6 (**H-I**) wild type (+/+) and *Nefl-Cre;Nfasc*^{Flox} mice. Longitudinal sections of the sciatic nerve (**A-I, N**) depict the organization of the axonal domains. (**J-M, O**) Transverse (cross) sections through the nodes of P15 wild type (+/+; **H**) and *Nefl-Cre;Nfasc*^{Flox} **(I-K, M**) sciatic nerves depict the arrangement of the nodal Schwann cell microvilli. Arrows mark the Schwann cell microvilli (**A-F, J-M**), the movement of the adjacent paranodal membranes (**I**), and constriction of the axonal membrane (**N**). Arrowheads highlight the electron-dense paranodal septae (**C-I, O**) and abnormal axonal membrane and organelle accumulation (**M**). Asterisks indicate invading Schwann cell microvilli (**G**) and the location of the node (**I**). Scale bars represent 0.5μm (**A-B, E-F, J-M**) and 0.2μm (**CD, G-I, N-O**). The “m” denotes the presence of mitochondria in the nodal region (**E, I**), and the “a” refers to the axon (**J-O**).

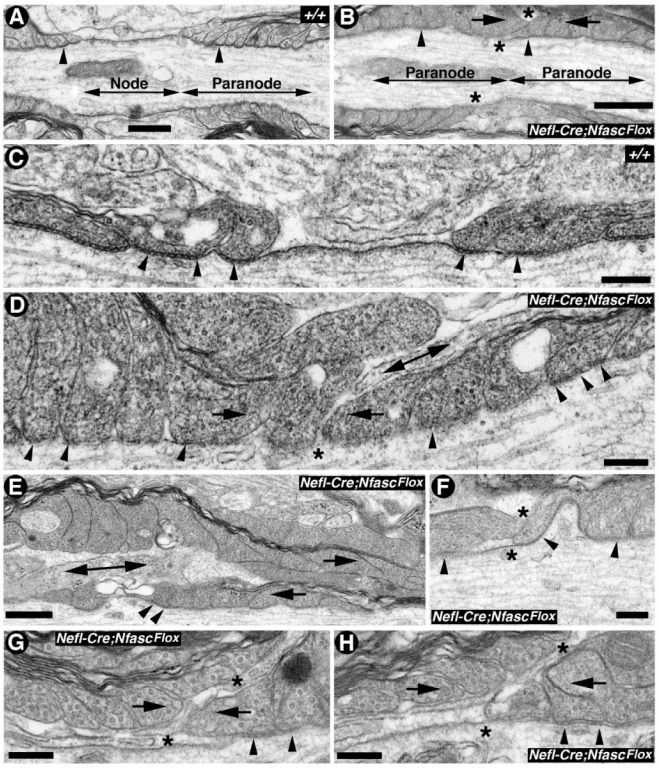

Figure 5. Proper nodal assembly is essential in preventing paranodal invasion in the CNS nodes

Electron micrographs of P15 (**A-B, E-H**) and P6 **(C-D**) wild type (+/+) and *Nefl-Cre;Nfasc*^{Flox} mice. Longitudinal sections of the cervical spinal cord of wild type (+/+, **A, C**) mice depict the typical organization of the nodal and paranodal regions of myelinated fibers compared to *Nefl-Cre;Nfasc*^{Flox} fibers **(B; D-H)**. Arrowheads mark the presence of paranodal axo-glial septate-like junctions. Asterisks mark the nodal region in *Nefl-Cre;Nfasc*^{Flox} myelinated fibers. Arrows indicate the direction of the paranodal loops **(B, D-H)**. The double arrows (**D-E)** denote the presence of a perinodal astrocytic process occupying the space between two invading paranodal domains. Scale bars represent 0.5μm **(A-B, E)** 0.2μm **(C-D, F-H**).

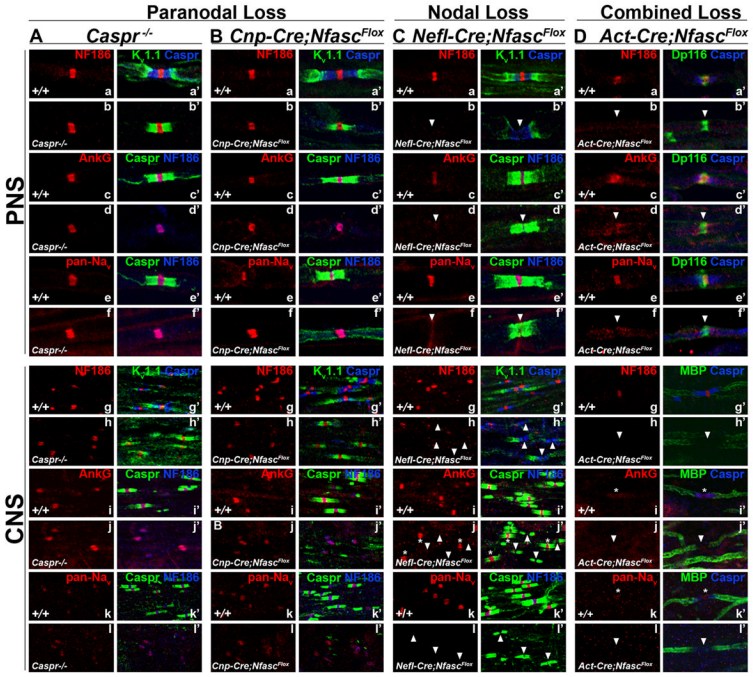

Figure 6. Node of Ranvier organization occurs independent of paranodal domains in the PNS and CNS myelinated axons

(A-D) Sciatic nerves (**a-f**) and spinal cords (**g-l**) from P19 *Caspr* null (*Caspr*$^{-/-}$; **A**), P15 *Nfasc*^{NF155} null (*Cnp-Cre;Nfasc*^{Flox}; **B**), P19 *Nfasc*^{NF186} null (*Nefl;Nfasc*^{Flox}; **C**), and P5 *Nfasc* null (*Act-Cre;Nfasc*^{Flox}; **D**) mice along with their age-matched wild type (+/+) littermates were immunostained with antibodies against NF186 (red in **A, B, C, D** at **a-b, g-h**, in all other panels NF186 is in blue), AnkG (red), and Na_v channels (pan-Na_v; red), as well as an array of domain specific markers as noted. In order to identify nodes in *Act-Cre;Nfasc*^{Flox} mice, immunostaining was carried out with antibodies against the nodal SC microvilli specific protein Dystrophin (Dp116) in sciatic nerves (PNS), and myelin basic protein (MBP, green) in CNS spinal cord fibers, plus Caspr (blue). Arrowheads mark the nodes lacking NF186 in both the *Nefl-Cre;Nfasc*^{Flox} and *Act-Cre;Nfasc*^{Flox} myelinated fibers. Asterisks denote the nodes still expressing NF186 in the *Nefl-Cre;Nfasc*^{Flox} spinal cords (**Cj-j′**). (See also Fig. S5).

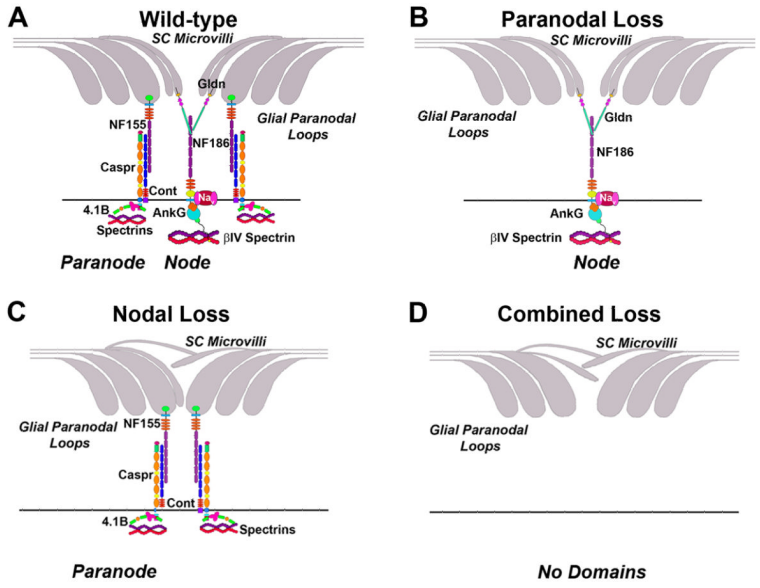

Figure 7. Organization and maintenance of molecular domains in PNS myelinated axons

Schematic diagram depicting key proteins involved in the organization and/or stabilization of axonal domains within myelinated fibers in the peripheral nervous system (PNS) (**A**), and the effects of paranodal **(B)**, nodal **(C)**, and combined domain **(D)** loss to the overall organization of axonal domains in myelinated fibers. $Nfasc^{NF186}$ (NF186) coordinates initial nodal organization by recruiting AnkG and voltage-gated sodium channels (Na_V) to nodes prior to the clustering of the paranodal components Caspr, $Nfasc^{NF155}$ (NF155), and contactin (Cont) **(A).** In the absence of intact paranodes in *Caspr* mutants **(B)**, clustering of the nodal components still occurs, and the complex is stabilized by the neuronal cytoskeleton in the PNS and CNS, as well as the association of NF186 with the nodal Schwann cell (SC) microvilli specific protein gliomedin (Gldn) in the PNS only. When NF186 expression is ablated, Na_V channels, AnkG, as well as the other nodal components fail to assemble, resulting in the lateral movement of the flanking paranodal domains into the nodal gap in the CNS and PNS. Continued invasion by the paranodal domains ultimately results in complete disorganization of the axonal domains within myelinated fibers, leading to severe conduction delays or complete loss of nerve conduction, as observed in mice lacking paranodal and nodal domains **(D)**.